Giant microcavity enhancement of second-harmonic generation in all-silicon photonic crystals

T. V. Dolgova, A. I. Maidykovski, M. G. Martemyanov, A. A. Fedyanin, and O. A. Aktsipetrov[a)]
Department of Physics, Moscow State University, 119992 Moscow, Russia

G. Marowsky
Laser-Laboratorium Goettingen, D-37077 Goettingen, Germany

V. A. Yakovlev
Institute of Spectroscopy, Russian Academy of Sciences, 142092 Troitsk, Russia

G. Mattei
Istituto di Metodologie Avanzate Inorganiche, CNR, 00016 Monterotondo Sc. Roma, Italy

(Received 18 March 2002; accepted 6 August 2002)

Second-harmonic generation (SHG) spectra of single and coupled porous silicon-based photonic crystal microcavities are studied in both frequency and wave vector domains. For the fundamental field resonant to the microcavity mode the second-harmonic intensity is enhanced by 10^2 times in comparison with that outside the photonic band gap. SHG spectroscopy in identical microcavities coupled through the intermediate Bragg reflector reveals two SHG peaks if the fundamental field is in resonance with the splitted mode of coupled microcavities. The spatial confinement of the resonant fundamental radiation is directly probed at the microcavity cleavage by scanning near-field optical microscopy. © *2002 American Institute of Physics.* [DOI: 10.1063/1.1510968]

One of the issues regarding the application of photonic crystals[1] is the control of the nonlinear-optical response enhancement in a preset spectral region.[2] For instance, the multiple reflection interference of forward- and backward-propagating waves can compensate the phase mismatch between the fundamental and second-harmonic (SH) waves and fulfills the phase-matching conditions in the spectral ranges of the edges of the photonic band gap (PBG).[3–7] Additional enhancement mechanism can be realized in the planar photonic crystal microcavities (MC) constituted of two Bragg reflectors separated by a submicron-thick spacer. The cavity mode located inside PBG manifests as a sharp drop at the high reflectivity plateau of the linear reflection spectrum. The optical field is strongly confined inside MC as the wavelength of the incident field is in resonance with the cavity mode. The recently observed enhancement of second-harmonic generation (SHG) in microcavities with a nonlinear spacer is due to the confinement of the SH[8,9] or fundamental[10] radiation between the linear Bragg reflectors or the metallic mirrors. The SHG enhancement is also obtained in MC with dual-wavelength nonperiodic Bragg reflectors[11] or with the spacer fabricated from a quasiphase-matching stack of alternating GaAs and AlAs layers.[12] Since the resonant optical field significantly expands into Bragg reflector the constructive SHG buildup in microcavities can be achieved if both the MC spacer and Bragg reflectors are composed from nonlinear materials. The SHG enhancement in this case arises from the combination of the phase mismatch compensation and the optical field confinement.

Macroporous and mesoporous silicon MC and photonic crystals[13,14] are attractive for all-silicon-based optoelectronic applications being easily incorporated in the semiconductor technology. Various optical effects such as the strong photoluminescence narrowing,[15] the Raman scattering enhancement,[16] the large birefringence,[17] and the giant third-harmonic generation[18] are recently observed in porous silicon (PS) microcavities and photonic crystals.

In this letter the experimental study of the SHG enhancement in all-silicon photonic crystal microcavities is presented. SHG spectroscopy in both frequency and wave vector domains reveals the giant SHG enhancement in mesoporous silicon MC. The resonant SHG enhancement is also observed in identical coupled microcavities.

The MC samples are fabricated by conventional electrochemical technique.[14] The peculiarities of the method are described in detail in Ref. 19. Briefly, the Si(001) wafer etching in the $HF:C_2H_5OH$ solution forms the mesoporous silicon layer. The PS layers with different porosity and thickness are obtained by the variation of the current density and the etching time. MC with the mode centered at the wavelength of λ_{MC} for normal incidence are composed from two Bragg reflectors separated by the $\lambda_{MC}/2$-thick MC spacer. Each Bragg reflector has 5 or 5.5 pairs of $\lambda_{MC}/4$-thick PS layers with two different refractive indices (porosities).

The output of a ns-OPO laser system is used as the fundamental radiation with wavelength λ_ω tunable from 730 to 1050 nm. The pulse duration is of 4 ns with the energy of 10 mJ per pulse and the spot diameter of 5 mm. The wave vector domain SHG spectroscopy is performed by tuning the angle of incidence θ of the 1064 nm output of a 10 ns yttritium–aluminum–garnet:Nd^{3+} laser[19] with energy of 6 mJ per pulse and spot diameter of 1 mm. The *s*-in, *p*-out polarization combination is chosen. For scanning near-field optical microscopy (SNOM) the MC cleavage perpendicular to the MC surface is placed onto 3-axes piezotube scanner and illuminated through the multimode fiber perpendicular to it. The fiber tip-sample distance is controlled by a shear force

a)Electronic address: aktsip@shg.ru

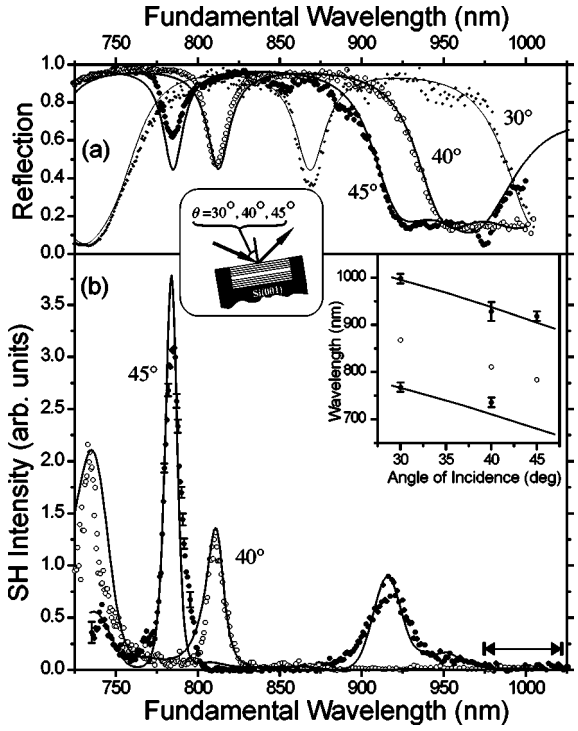

FIG. 1. (a). The linear reflection spectra of the PS microcavity measured for various angles of incidence. (b). The SHG spectra for $\theta=45°$ (filled circles) and $\theta=40°$ (open circles). Curves are the result of the combined fit to linear reflection and SHG spectra. Inset: The angular dependence of positions of SHG peaks at the MC mode (open circles) and the PBG edges (filled circles), and the calculated angular dependences of the PBG edges (lines).

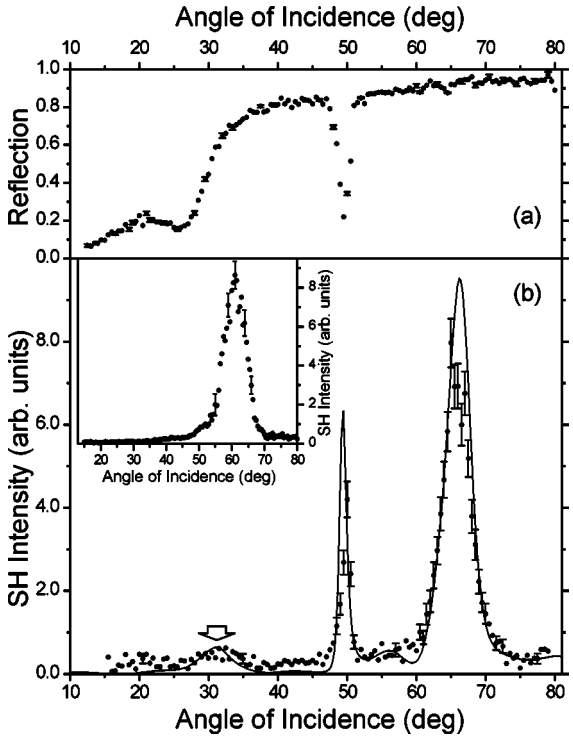

FIG. 2. (a) The angular spectrum of the *s*-polarized fundamental wave reflected from MC with $\lambda_{MC}=1350$ nm. (b). The SHG angular spectrum of this MC. Arrow emphasizes the SHG peak at the low-angle PBG edge. Curve is the result of the model calculations. Inset. The SHG angular spectrum of the photonic crystal with $\lambda_{PC}=1200$ nm.

feedback system. SNOM works in the collection mode, the light confined in the sample is collected into the fiber tip.

Figure 1(a) shows the linear spectra of the *s*-polarized fundamental radiation reflected from MC with $\lambda_{MC}=945$ nm. The spectra have the plateau with almost full reflection corresponded to PBG and the dip related to the MC mode. Figure 1(b) shows the SH intensity spectra acquired for this MC. The SH intensity is strongly enhanced at $\lambda_\omega \simeq 785$ nm for $\theta=45°$ and at $\lambda_\omega \simeq 810$ nm for $\theta=40°$ as the fundamental field is in resonance with the mode, i.e., if $\lambda_\omega = \lambda_{MC}\sqrt{1-n_{MC}^{-2}\sin^2\theta}$, where n_{MC} is refractive index of the MC spacer. The largest enhancement is detected for $\theta=45°$ and is 130 times in comparison with that averaged outside PBG in the λ_ω interval from 975 to 1025 nm and indicated in Fig. 1(b) by the arrow. Two other spectral features at $\lambda_\omega \simeq 915$ nm for $\theta=45°$ and at $\lambda_\omega \simeq 735$ nm for $\theta=40°$, respectively, correspond to both PBG edges. As θ decreases to 30°, SHG peaks redshift [inset of Fig. 1(b)] in accordance with the angular dependence of the spectral positions of the PBG edges and the MC mode. The large difference in the magnitude of the SHG peaks at the PBG edges for $\theta=40°$ is most likely associated with the two-photon resonance of PS quadratic susceptibility related to the E_0'/E_1 critical point of the crystalline silicon band structure.

The MC confinement of the fundamental field is also achieved by tuning the angle of incidence of the fundamental radiation with the fixed λ_ω. Figures 2(a) and 2(b) show the angular spectra of the linear reflection coefficient at $\lambda_\omega = 1064$ nm and the SH intensity, respectively, acquired for MC with $\lambda_{MC}=1350$ nm. The SHG angular spectrum has a narrow peak at $\theta \simeq 50°$ corresponded to the dip in the linear reflection spectrum and attributed to the fundamental field resonance with the MC mode. The two broader peaks at 30° and 65° are related to the PBG edges. The edge at large θ values is unresolved in Fig. 2(a) due to the strong angular dependence of the Fresnel factors. However, the SHG angular spectrum of the other PS photonic crystal with PBG centered at $\lambda_{PC}=1200$ nm for normal incidence [inset of Fig. 2(b)] reveals a peak with the similar angular width and position to the SHG peak at 65° for MC. The different magnitude of the SHG peaks at the PBG edges is a result, in part, of the the angular dependence of the isotropic SHG component.[20] The calibration of the resonant SHG signal from MC is performed using the Si(001) substrate. The SH intensity in the maximum of the SHG angular spectrum measured at this silicon surface in a *p*-in, *p*-out polarization combination is at least 150 times smaller.

The SHG spectra are approximated using the nonlinear transfer matrix formalism,[21] which can be used for description of SHG in periodic media among a Green's function approach.[22] The peculiarities of the model and details of the fit are presented in the forthcoming article.[19] Curves in Figs. 1 and 2 show the results of the least-square fit to the SHG spectra and demonstrate a good agreement with the data. The SHG resonance at the MC mode is caused by the spatial confinement of the fundamental field inside the spacer and the constructive interference of complex SHG contributions from each PS layer which accounts for the phase-matching in the periodic MC structure.[19] The SHG enhancement at the PBG edges is due to the phase matching and the slight homogeneous fundamental field amplification inside MC.[6,7,19]

Figure 3 shows the topographical and resonant SNOM images acquired at the MC cleavage. The topographical image shows the high MC lateral quality and periodicity. The

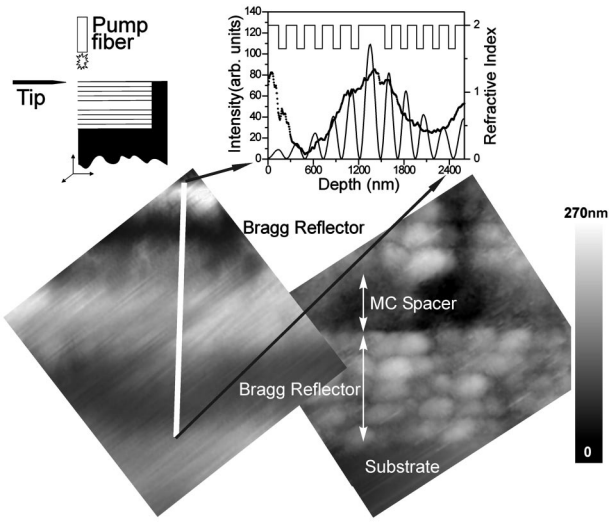

FIG. 3. Resonant SNOM (left) and topographical (right) images of the cleavage of MC with $\lambda_{MC}=620$ nm. Inset. The cross section of the intensity distribution extracted from the SNOM image (dots) and calculated within transfer matrix formalism (line). Rectangular curve shows the profile of the real part of the PS layers refractive index at 633 nm.

SNOM image obtained for the 633 nm-pump radiation demonstrates the bright strip in the vicinity of the MC spacer surrounded by dark bands corresponded to Bragg reflectors. The contrast between maximum and minimum of intensity is $\simeq 10$ and describes the field localization degree. The cross section conforms good to the envelope of calculated intensity distribution. The fine structure of the intensity distribution with the period of the standing wave is not resolved. This implies that the apertureless tip detects the field scattered by the neighboring PS layers, loosing the fine lateral resolution. The increase of the intensity at the surface area below 200 nm is more likely caused by sample surface scattering of the pump radiation.

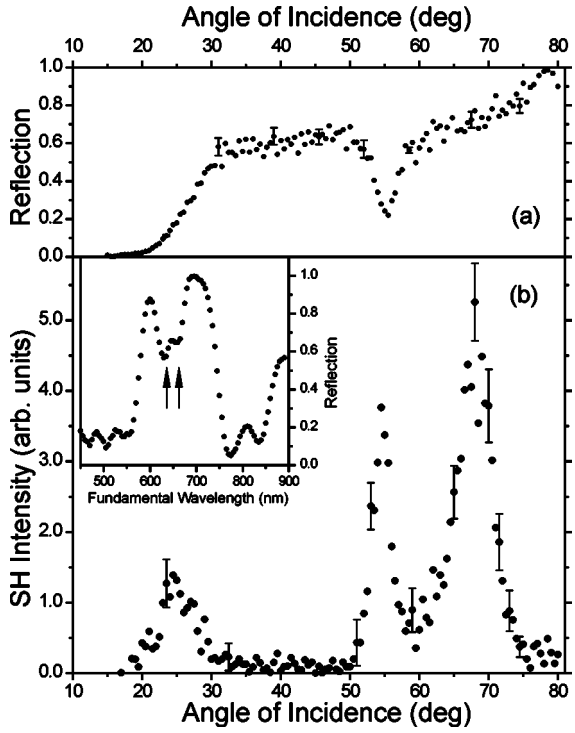

FIG. 4. (a) The angular spectrum of the *s*-polarized radiation of 1064 nm reflected from coupled MC with $\lambda_{MC}=1250$ nm. (b). The SHG angular spectrum of this MC. Inset. The spectrum of the linear reflection coefficient of coupled MC with $\lambda_{MC}=680$ nm. Arrows indicate positions of the splitted cavity modes.

Further, the SHG spectrum is measured for the sample with the two identical $\lambda_{MC}/2$-thick spacers separated by the intermediate semitransparent Bragg reflector. Figure 4(b) shows the SHG angular spectrum of coupled MC with $\lambda_{MC}=1250$ nm. The spectrum has the peak at $\theta\simeq 25°$ coinciding with the PBG edge and two resonances at approximately 55° and 67° corresponding to splitted modes of coupled MC. The SHG resonance at 55° correlates with the dip in the fundamental field reflection spectrum [see Fig. 4(a)]. The second mode of coupled MC at 67° is unresolved in linear spectrum due to the strong angular dependence of the Fresnel factors. However, the linear reflection spectrum measured in the frequency domain at the similar coupled MC sample proves the presence of split modes.

In conclusion, SHG spectroscopy in all-silicon photonic crystal microcavities is reported. The fundamental field confinement in the microcavity spacer combined with the phase matching in the periodic MC structure causes the giant SHG enhancement if the fundamental wave resonance with the cavity mode. The simplicity of the mode tuning and the possibility of the integration of all-silicon microcavities in semiconductor technology highlight their potential use for integrated optics applications including optical sensors and frequency converters.

[1] J. Joannopoulos, R. Meade, and J. Winn, *Photonic Crystals* (Prinston University Press, Princeton, NJ, 1995).
[2] K. Sakoda, *Optical Properties of Photonic Crystals* (Springer, Berlin, 2001).
[3] N. Bloembergen and J. Sievers, Appl. Phys. Lett. **17**, 483 (1970).
[4] J. P. van der Ziel and M. Ilegems, Appl. Phys. Lett. **28**, 437 (1976).
[5] M. J. Steel and C. M. de Sterke, Appl. Opt. **35**, 3211 (1996).
[6] M. Scalora, M. J. Bloemer, A. S. Manka, J. P. Dowling, C. M. Bowden, R. Viswanathan, and J. W. Haus, Phys. Rev. A **56**, 3166 (1997).
[7] A. V. Balakin, V. A. Bushuev, B. I. Mantsyzov, I. A. Ozheredov, E. V. Petrov, A. P. Shkurinov, P. Masselin, and G. Mouret, Phys. Rev. E **63**, 046609 (2001).
[8] J. Trull, R. Vilaseca, J. Martorell, and R. Corbalan, Opt. Lett. **20**, 1746 (1995).
[9] V. Pellegrini, R. Colombelli, I. Carusotto, F. Beltram, S. Rubini, R. Lantier, A. Franciosi, C. Vinegoni, and L. Pavesi, Appl. Phys. Lett. **74**, 1945 (1999).
[10] H. Cao, D. B. Hall, J. M. Torkelson, and C.-Q. Cao, Appl. Phys. Lett. **76**, 538 (2001).
[11] C. Simonneau, J. P. Debray, J. C. Harmand, P. Vidakovic, D. J. Lovering, and J. A. Levenson, Opt. Lett. **22**, 1775 (1997).
[12] S. Nakagawa, N. Yamada, N. Mikoshiba, and D. E. Mars, Appl. Phys. Lett. **66**, 2159 (1995).
[13] S. W. Leonard, H. M. van Driel, K. Busch, S. John, A. Birner, A.-P. Li, F. Müller, U. Gösele, and V. Lehmann, Appl. Phys. Lett. **75**, 3063 (1999).
[14] L. Pavesi, Riv. Nuovo Cimento **20**, 1 (1997).
[15] V. Pellegrini, A. Tredicucci, C. Mazzoleni, and L. Pavesi, Phys. Rev. B **52**, R14328 (1995).
[16] L. A. Kuzik, V. A. Yakovlev, and G. Mattei, Appl. Phys. Lett. **75**, 1830 (1999).
[17] F. Genereux, S. W. Leonard, H. M. van Driel, A. Birner, and U. Gösele, Phys. Rev. B **63**, 161101 (2001).
[18] T. V. Dolgova, A. I. Maidikovsky, M. G. Martemyanov, A. A. Fedyanin, and O. A. Aktsipetrov, JETP Lett. **75**, 15 (2002) [Pis'ma Zh. Eksp. Teor. Fiz. **75**, 17 (2002)].
[19] T. V. Dolgova, A. I. Maidikovsky, M. G. Martemyanov, A. A. Fedyanin, O. A. Aktsipetrov, D. Schuhmacher, G. Marowsky, V. A. Yakovlev, G. Mattei, N. Okta, and S. Nakabayashi, J. Opt. Soc. Am. B **19**, 2129 (2002).
[20] N. Bloembergen, R. K. Chang, S. S. Jha, and C. H. Lee, Phys. Rev. **174**, 813 (1968).
[21] D. S. Bethune, J. Opt. Soc. Am. B **6**, 910 (1989).
[22] J. E. Sipe, J. Opt. Soc. Am. B **4**, 481 (1987).